THE JOURNAL OF BIOLOGICAL CHEMISTRY VOL. 292, NO. 10, pp. 4138–4151, March 10, 2017

Biochemical and Cellular Analysis Reveals Ligand Binding Specificities, a Molecular Basis for Ligand Recognition, and Membrane Association-dependent Activities of Cripto-1 and Cryptic*

Received for publication, July 12, 2016, and in revised form, January 25, 2017 Published, JBC Papers in Press, January 26, 2017, DOI 10.1074/jbc.M116.747501

Senem Aykul, Anthony Parenti, Kit Yee Chu, Jake Reske, Monique Floer, Amy Ralston, and Erik Martinez-Hackert[1]
From the Department of Biochemistry and Molecular Biology, Michigan State University, East Lansing, Michigan 48824-1319

Edited by Norma Allewell

Transforming growth factor β (TGF-β) pathways are key determinants of cell fate in animals. Their basic mechanism of action is simple. However, to produce cell-specific responses, TGF-β pathways are heavily regulated by secondary factors, such as membrane-associated EGF-CFC family proteins. Cellular activities of EGF-CFC proteins have been described, but their molecular functions, including how the mammalian homologs Cripto-1 and Cryptic recognize and regulate TGF-β family ligands, are less clear. Here we use purified human Cripto-1 and mouse Cryptic produced in mammalian cells to show that these two EGF-CFC homologs have distinct, highly specific ligand binding activities. Cripto-1 interacts with BMP-4 in addition to its known partner Nodal, whereas Cryptic interacts only with Activin B. These interactions depend on the integrity of the protein, as truncated or deglycosylated Cripto-1 lacked BMP-4 binding activity. Significantly, Cripto-1 and Cryptic blocked binding of their cognate ligands to type I and type II TGF-β receptors, indicating that Cripto-1 and Cryptic contact ligands at their receptor interaction surfaces and, thus, that they could inhibit their ligands. Indeed, soluble Cripto-1 and Cryptic inhibited ligand signaling in various cell-based assays, including SMAD-mediated luciferase reporter gene expression, and differentiation of a multipotent stem cell line. But in agreement with previous work, the membrane bound form of Cripto-1 potentiated signaling, revealing a critical role of membrane association for its established cellular activity. Thus, our studies provide new insights into the mechanism of ligand recognition by this enigmatic family of membrane-anchored TGF-β family signaling regulators and link membrane association with their signal potentiating activities.

The mammalian "epidermal growth factor-Cripto/FRL-1/Cryptic" (EGF-CFC)[2] family proteins Cripto-1 and Cryptic are membrane-anchored regulators of TGF-β family signaling that have key roles in early embryonic development (1–6). Cripto-1 (also known as TDGF1) is a marker of stem cell pluripotency that is implicated in embryonic patterning (7–11). Cryptic (also known as CFC1) is associated with heart morphogenesis and left-right asymmetry specification (12–14). Biological functions beyond embryogenesis are not known, but both play major roles in human diseases. Cripto-1 is associated with colon, breast, pancreatic, ovarian, lung, and other cancers (15–18). Cryptic is associated with heterotaxy syndromes and other laterality defects (19–21).

Molecular genetic studies have established a functional link between Cripto-1 and the TGF-β family ligand Nodal (4, 22): Nodal co-immunoprecipitated with Cripto-1 and required Cripto-1 for signaling (9, 13, 23–29). These findings have supported the idea that Cripto-1 and the EGF-CFC family are obligate Nodal "co-receptors" that potentiate Nodal signaling (3, 30, 31). However, the fundamental requirement of Cripto-1 for this function is not certain, as some studies indicated that Nodal can bind its receptors and can have signaling activities without Cripto-1 (8, 25–27, 32, 33). Intriguingly, a number of studies discovered a seemingly contradicting function. Namely, Cripto-1 blocked signaling by the TGF-β family ligands Activin A, Activin B, and TGF-β1, indicating Cripto-1 could also act as antagonist of some ligands (28, 34–36). Together, these findings indicate that the function of Cripto-1 remains unclear. Although Cripto-1 has been widely investigated, less is known about Cryptic, except that it is also implicated in Nodal signaling (13, 29, 30).

To clarify the functions of Cripto-1 and Cryptic, we examined their molecular mechanisms in TGF-β family signaling. Using purified proteins expressed in mammalian cells and protein-protein interaction analysis, we showed human Cripto-1 binds Nodal as expected, but not Activin A or Activin B as previously suggested. Notably, we discovered Cripto-1 also binds BMP-4 with high affinity, revealing a new regulatory function. By contrast, mouse Cryptic only bound Activin B, indicating its biological activities are different from Cripto-1.

* This work was supported by the Michigan State University, the Clinical and Translational Sciences Institute, and National Institutes of Health Grants R41 AR068804, R43 CA203180, and R01 GM104009 (to A. R.). S. A., E. M. H., and Michigan State University have filed a patent application on the use of Cripto-1/Cryptic as inhibitors. The content is solely the responsibility of the authors and does not necessarily represent the official views of the National Institutes of Health.
[1] To whom correspondence should be addressed: Rm. 509, 603 Wilson Rd., East Lansing, MI 48824-1319. Tel.: 517-355-1604; E-mail: emh@msu.edu.
[2] The abbreviations used are: EGF-CFC, epidermal growth factor-Cripto/FRL-1/Cryptic; XEN, extraembryonic endoderm stem; GPI, glycosylphosphatidylinositol; SEC, size exclusion chromatography; BMP, bone morphogenetic protein; PNGase F, peptide *N*-glycosidase F; RU, response unit; RLU, *Renilla* luciferase units; VE, visceral endoderm; RGM, repulsive guidance molecule.

We also investigated how Cripto-1 and Cryptic recognize ligands. Using a surface plasmon resonance competition assay (37), we discovered both Cripto-1 and Cryptic inhibited ligand-receptor binding, indicating they contact the type I and type II receptor recognition surfaces on ligands (38). As both Cripto-1 and Cryptic blocked ligand-receptor binding, we speculated they could inhibit signaling. Using reporter gene expression assays, and an extraembryonic endoderm stem (XEN) cell differentiation assay (39, 40), we demonstrated that soluble forms of Cripto-1 and Cryptic, respectively, inhibited BMP-4 and Activin B signaling in a cellular context. But in agreement with earlier reports on the role of Cripto-1 in Nodal function, membrane-bound Cripto-1 potentiated BMP-4 signaling. This finding reveals a potentially critical role for membrane association in signal potentiation. In summary, we provide a molecular framework that helps explain the function of these enigmatic TGF-β family signaling regulators. Although soluble Cripto- 1 and Cryptic can act as inhibitors, membrane-anchored forms could exploit this ligand capture function and localize ligands to endosomal vesicles as a way to potentiate signaling (41, 42).

Results

Production of Soluble Cripto-1 and Cryptic—A critical bottleneck in the molecular analysis of mammalian Cripto-1 and Cryptic has been the lack of purified, active proteins. Several complicating factors contribute to this problem. Both Cripto-1 and Cryptic are expressed as secreted precursors that attach to the membrane via a glycosylphosphatidylinositol (GPI) anchor, both have six disulfide bonds distributed between two separate domains, and both may require post-translational fucosylation for biological activity (5, 43–45). To obtain active Cripto-1 and Cryptic we used stably transfected Chinese hamster ovary (CHO) cells, as they can carry out the required post-translational modifications. We created a Cripto-1 expression construct that included the Cryptic signal peptide and human Cripto-1 extracellular (ecto)-domain amino acids 31–163. We also created a mouse Cryptic expression construct that included the native signal peptide plus ectodomain amino acids 36–175 (Fig. 1*A*). Both fragments were fused at their C terminus, which is near the predicted GPI processing site, to human IgG1 Fc (Fig. 1, *A* and *B*). Fusion proteins were purified from conditioned medium by protein A affinity capture. A size exclusion chromatography (SEC) step was further required to remove inactive aggregates (Fig. 1*C*). Overall, we obtained approximately ~100 mg of highly purified hCripto-1-Fc and ~50 mg of mCryptic-Fc/liter of culture. Notably, the C terminus was critical for expression, as constructs that ended near the C-terminal cysteine were highly aggregated, and constructs that ended at the putative GPI processing site failed to secrete.

Cripto-1 and Cryptic Bind Distinct Ligands—Genetic and co-immunoprecipitation studies have indicated that Cripto-1 and Cryptic interact with the TGF-β family ligands Nodal and Activin A (9, 13, 28, 35). Using SPR we confirmed earlier that Cripto-1 binds Nodal with high affinity (33), but we did not detect Activin A binding to Cripto-1 or Nodal binding to Cryptic. These findings indicated that previously proposed ligand-binding and regulatory activities of Cripto-1 and Cryptic are inaccurate. To identify ligands that interact directly with (and thus are regulated by) Cripto-1 or Cryptic, we used a high-throughput, SPR-based binding assay. We captured purified human Cripto-1-Fc or mouse Cryptic-Fc on an SPR sensor chip cross-linked with an anti-Fc antibody and injected 17 different TGF-β family ligands at an 80 nM concentration (Fig. 2, *A* and *B*). Cripto-1-Fc bound Nodal and, to a lesser degree GDF-3, but not Activin A, as had been proposed. Notably, we discovered that Cripto-1-Fc interacts very strongly with BMP-4 (Fig. 2*A*). By contrast, mouse Cryptic-Fc did not bind Nodal, Activin A, BMP-4, or GDF-3, but interacted very specifically and strongly with Activin B (Fig. 2*B*). We did not observe appreciable binding of any other tested TGF-β family ligand to either Cripto-1 or Cryptic, including TGF-β1, TGF-β2, TGF-β3, GDF-8, GDF-11, GDF-15, BMP-2, BMP-3, BMP-6, BMP-7, BMP-9, or BMP-10. We confirmed our single injection findings with systematic ligand titrations and obtained kinetic rate and equilibrium binding constants for BMP-4, GDF-3, and Activin B (Fig. 2, *C–F*, Table 1). To determine whether the Fc moiety affects ligand binding, we cross-linked Fc-free Cripto-1 directly on the sensor chip. Notably, Cripto-1 captured in this way bound BMP-4 with ~40-fold lower affinity, indicating that the Fc moiety or the capture method impact ligand binding (Fig. 2, *C* and *D*). We speculate three factors could contribute to the difference in affinity: 1) a loss of avidity due to use of the Fc-free, monomeric form; 2) a loss in binding activity due to chemical modification of lysine residues on Cripto-1; and/or 3) a gradual loss in binding activity caused by repeated regeneration of the Cripto-1 bound surface. Despite the observed differences in binding rates, our findings show that Cripto-1 binds BMP-4 with high affinity regardless of capture method. In conclusion, we have identified two new TGF-β family ligands that are bound (and thus regulated) by Cripto-1 or Cryptic, namely BMP-4 and Activin B. Importantly, we show Cripto-1 and Cryptic interact with different ligands, indicating they have markedly distinct biological functions.

All Cripto-1 Domains Are Required for Ligand Binding—EGF-CFC family proteins comprise three structural domains, an N-terminal low homology region (N), an epidermal growth factor (E)-like motif, and a C-terminal Cripto-FRL1-Cryptic (C) domain (Fig. 1*A*). The molecular functions of individual domains have been investigated, but results are inconclusive. For example, some studies indicate the EGF domain is required for signaling, whereas others suggest it is not (26, 30). Some indicate the EGF domain binds Nodal, whereas others indicate it does not (30, 42, 46). Some suggest the CFC domain interacts with ALK4, whereas others indicate it may not (26, 30). To clarify the contribution of Cripto-1 domains in ligand interactions, we created constructs that consisted of two domains (NE, EC, and NC) or single domains (N, E, or C) and compared their ability to bind ligands with that of full-length Cripto-1-Fc (NEC). We expressed and purified the six domain deletion constructs as described for the full-length form, and tested their ability to bind BMP-4 using single injection SPR binding. Of the six constructs, five were readily expressed and purified. The N-terminal domain construct (N) was severely degraded and thus was not used in these studies. Both two-domain constructs that included the EGF region (NE and EC) bound BMP-4, although binding was significantly weaker compared with full-

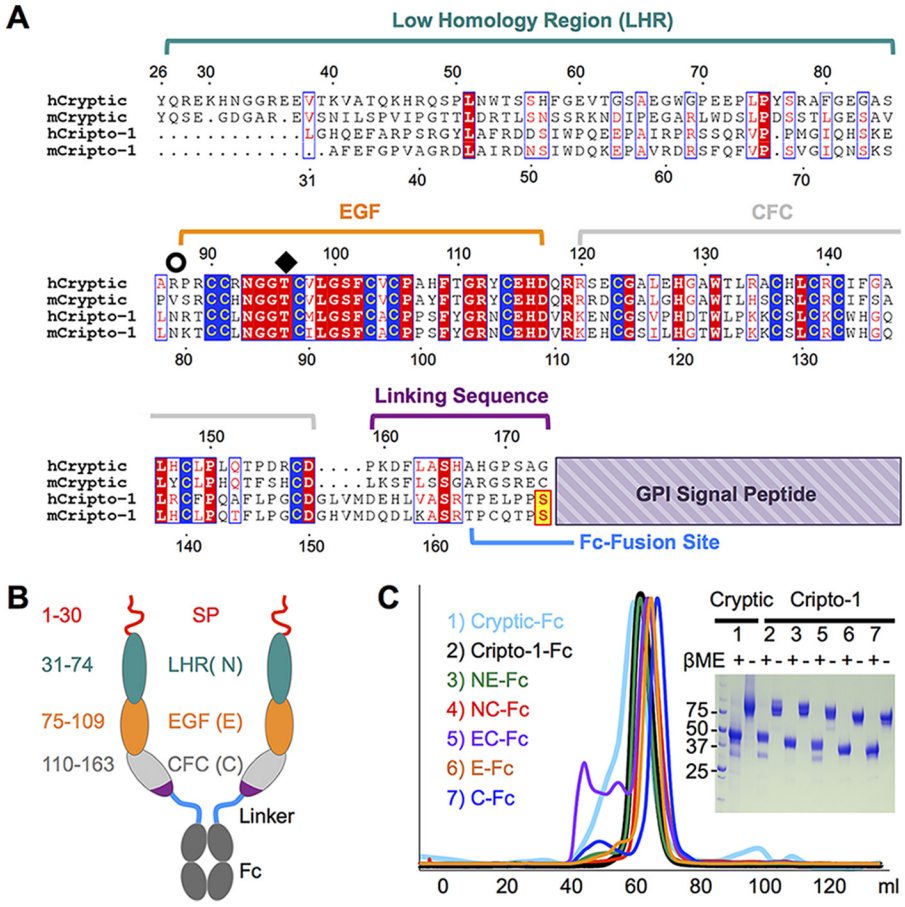

FIGURE 1. **Construct design and purification.** *A,* multiple sequence alignment of human and mouse Cryptic and Cripto-1. Both molecules have a signal peptide for secretion (not shown in the alignment), a low homology region (*LHR, teal*), an epidermal growth factor-like domain (*EGF, orange*), a Cripto-1-FRL-Cryptic domain (*CFC, gray*), and a GPI signal peptide (represented by the *purple box*). The Cripto-1 GPI signal peptide is cleaved after Ser-169 (residues in *yellow box*). Cryptic of mouse origin has a canonical GPI signal peptide, whereas Cryptic of primate origin has a large, non-canonical GPI signal peptide. The GPI modification site of Cryptic is not known. For expression constructs, human Cripto-1 and mouse Cryptic were truncated at the "Fc-Fusion site" (*light blue*). The *open circle* marks the *N*-linked glycosylation site. The *black diamond* marks the *O*-linked fucosylation site. Numbering represents amino acid positions of human Cryptic (*top*) and human Cripto-1 (*bottom*). *B,* domain organization of Cryptic/Cripto-1 constructs colored as in *A*. Both were fused to human Igg1-Fc via a 22-amino acid linker at the Fc-Fusion site. Numbering represents amino acid positions of human Cripto-1. *C,* purification of Cripto-1-Fc and Cryptic-Fc fusion forms expressed in CHO cells. Fc-fusion form constructs were captured from conditioned medium using protein A affinity chromatography and further purified using size exclusion chromatography. Constructs migrate as a single, well defined peak in a size exclusion chromatographic column. The molecular weight of the protein corresponds to the dimeric species. Non-reducing and reducing SDS-PAGE gels show the disulfide-linked dimeric species and the reduced, monomeric species. Dimerization occurs via free a cysteine in the Fc region.

length Cripto-1-Fc (Fig. 2*G*). Single domain constructs did not bind BMP-4. Taken together, these findings indicate that all three Cripto-1 domains are required for the BMP-4 interaction. However, whether all three domains contact BMP-4 directly or whether they help support a Cripto-1 conformation that recognizes BMP-4, remains to be determined. We did not test Cripto-1 domain functions against Nodal, as we do not have consistently active Nodal (Fig. 2*A*). But we expect Nodal to parallel our BMP-4 findings.

Cripto-1 Glycosylation Is Necessary for Ligand Binding—Human Cripto-1 is glycosylated at asparagine 79. This glycosylation site appears to be conserved across all mammalian species (Fig. 1*A*), indicating the glycan moiety may have functional relevance. To determine whether Asn-79 glycosylation has a role in ligand binding, we enzymatically processed Cripto-1 with the endoglycosidases PNGase F or ENDO-F3. PNGase F removes the entire glycan. ENDO-F3 leaves the *N*-acetylglucosamine moiety on the protein. Strikingly, both PNGase F- and ENDO-F3-treated Cripto-1-Fc lost the ability to bind BMP-4, indicating that Asn-79 glycosylation is critical for Cripto-1 function (Fig. 2*H*). Importantly, this finding supports our conclusion that Cripto-1-ligand recognition requires multiple structural features. However, whether Asn-79 glycosylation is directly involved in ligand binding or whether it plays a structural role remains to be determined. Notably, Asn-79 is at the junction between N and E domains. Only three of our domain constructs, NE, EC, and E, carried this glycosylation site. NE and EC constructs also lose their binding activity after deglycosylation (Fig. 2*H*).

Soluble Cripto-1 Does Not Bind Type I Receptors with High Affinity—The commonly accepted model of Cripto-1 action is that it binds both Nodal and the type I TGF-β family receptor ALK4 to stabilize Nodal·ALK4 complexes and thus potentiate Nodal signaling (26, 30, 46, 47). Specifically, it is suggested the EGF domain contacts Nodal and the CFC domain contacts ALK4, thus linking Nodal with its type I receptor and stabilizing an active signaling complex (48, 49). But our findings show the function of Cripto-1 is more complex. Namely, ligand binding

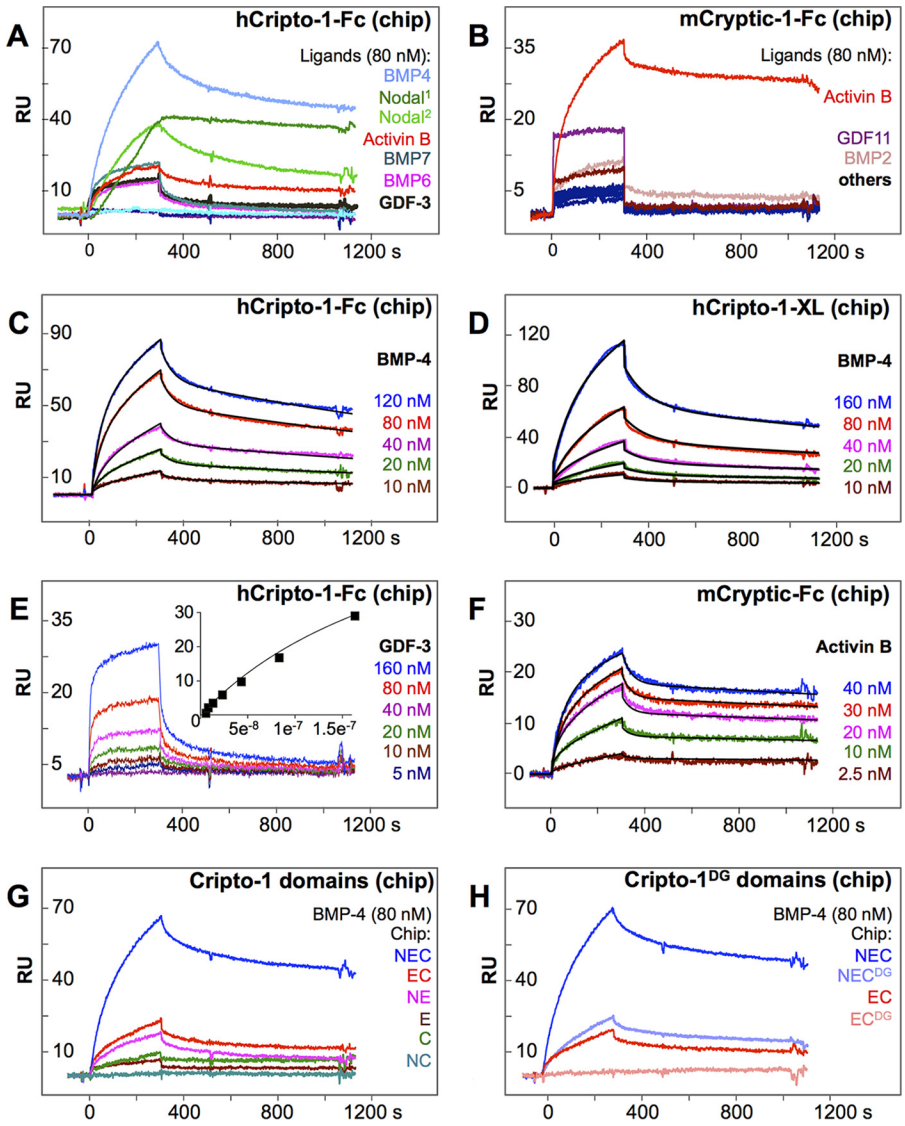

FIGURE 2. **Ligand binding specificity.** Approximately 250 RU of (*A*) Cripto-1-Fc or (*B*) Cryptic-Fc were captured on an SPR sensor chip, and 80 nM Activin A, Activin B, GDF-1, GDF-3, GDF-8, GDF-11, GDF-15, TGF-β1, TGF-β2, TGF-β3, BMP-2, BMP-3, BMP-4, BMP-6, BMP-7, BMP-9, BMP-10, or Nodal (lot 1 and lot 2) were injected. Ligands that elicited an SPR response are shown in relevant panels. Ligand name and corresponding binding curves are color-matched. *C,* human Cripto-1-Fc was captured on the sensor chip, and different concentrations of BMP-4 were injected. Colors of injection curves are matches with corresponding concentrations. *D,* human Cripto-1 was cross-linked to the sensor chip, and different concentrations of BMP-4 were injected. Colors of injection curves are matches with corresponding concentrations. *E,* human Cripto-1-Fc was captured on the sensor chip, and different concentrations of GDF-3 were injected. Colors of injection curves are matches with corresponding concentrations. The *inserted panel* shows the equilibrium-binding analysis. *F*, mouse Cryptic-Fc was captured on the sensor chip, and different concentrations of Activin B were injected. Colors of injection curves are matches with corresponding concentrations. Fitted curves (*black lines*) are superimposed over all experimental curves. Calculated binding rate constants and equilibrium dissociation rate constants are shown in Table 1 (*C-F*). *G,* Cripto-1-Fc domain deletion constructs were captured on the sensor chip and 80 nM BMP-4 was injected. Cripto-1 constructs are named according to their domain composition, *i.e. N* constructs have the N-terminal low homology region, *E* constructs have the EGF domain, and *C* constructs have the CFC domain. Injection curves are color-matched with corresponding constructs. *H*, glycosylated and deglycosylated (*DG*) full-length Cripto-1 (*NEC*) and the N-terminal domain deletion construct (*EC*) were captured on the sensor chip and 80 nM BMP-4 was injected. Injection curves are color-matched with corresponding constructs and glycosylation status.

TABLE 1
Binding rate and equilibrium dissociation constants

Analyte	Chip	k_a[a]	k_d	K_d	Chi^2	R^2
BMP-4	Cripto-1-Fc	8.390×10^4	4.000×10^{-4}	4.770	0.710	
BMP-4	Cripto-1-XL	1.930×10^4	3.650×10^{-3}	189	1.490	
GDF-3	Cripto-1-Fc			256	0.637	
Activin B	mCryptic-Fc	1.260×10^4	1.410×10^{-4}	1.120	0.221	
ALK4	Cripto-1-Fc	ND[b]	ND	1307		0.989
ALK4	Cripto CFC-Fc	ND	ND	750.4		0.996
Cripto-1	ALK4-Fc	ND	ND	725.2		0.998

[a] Units are: k_a ($M^{-1}s^{-1}$), k_d (s^{-1}), K_d (nM), Chi^2 (RU^2).
[b] ND, not determined.

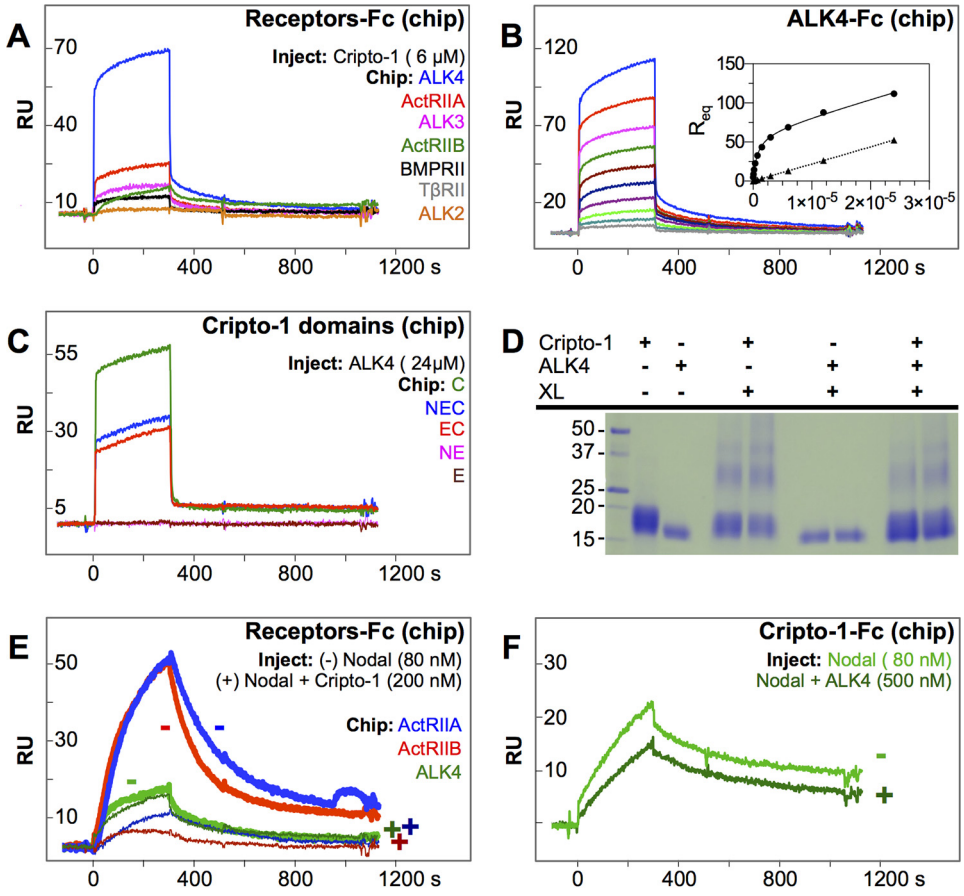

FIGURE 3. **Cripto-1 and Cryptic-receptor interactions.** *A,* binding of Cripto-1 to TGF-β family receptors. Type I receptors ALK2-Fc, ALK3-Fc, and ALK4-Fc, or type II receptors ActRIIA-Fc, ActRIIB-Fc, BMPRII-Fc, and TβRII-Fc were captured on the sensor chip. 6 μM Fc free Cripto-1 or Cryptic was injected. Receptors and corresponding binding curves are color-matched. Cryptic binding curves are not shown, as Cryptic did not elicit an SPR response. *B,* ALK4-Cripto-1 interaction analysis. ALK4-Fc was captured and Fc free Cripto-1 was injected at concentrations of 24.0 μM (*blue*), 12.0 μM (*red*), 6.0 μM (*magenta*), 3.0 μM (*green*), 1.5 μM (*maroon*), 750.0 nM (*dark blue*), 375.0 nM (*purple*), 187.5 nM (*light green*), 93.75 nM (*teal*), and 46.875 nM (*gray*). Equilibrium binding analysis does not fit a standard Langmuir model. Instead, nonlinear curve fitting using a "one-site total binding" model was used (*inset, solid line, circles*). B_{max}, K_d, and nonspecific contribution were determined. The theoretically determined nonspecific contribution is also shown (*inset, dotted line, triangles*). *C,* binding of ALK4 to Cripto-1 domain deletion constructs. Deletion constructs were captured on the sensor chip and 6 μM Fc free ALK4 was injected. Constructs and corresponding binding curves are color-matched. *D,* glutaraldehyde cross-linking of Cripto-1 and ALK4. The SDS-PAGE gel shows Cripto-1, ALK4, cross-linked (*XL*) Cripto-1, cross-linked ALK4, and cross-linked complexes. 0.01% (*left lane*) and 0.02% (*right lane*) glutaraldehyde was used. Molecular weight markers are shown on the *left side*. *E,* binding of Nodal ± Cripto-1 to Nodal receptors ActRIIA (*blue*), ActRIIB (*red*), and ALK4 (*green*). The *minus sign* denotes curves obtained with Nodal only (*thick, light colored lines*), the *plus sign* denotes curves obtained with Nodal preincubated with Cripto-1 (*thin, dark colored lines*). A Cripto-1 injection over captured ALK4 was subtracted from the Nodal·Cripto-1 injection over captured ALK4 to eliminate the nonspecific Cripto-1·ALK4 binding contribution. *F,* binding of Nodal ± ALK4 (*green*) to Cripto-1. The presence of ligand does not appear to alter the SPR signal obtained for Cripto-1 and ALK4 significantly.

necessitates all three domains, including the CFC domain (Fig. 2*G*). To investigate the function of Cripto-1 in ligand-receptor complex stabilization, we first examined if Cripto-1 binds TGF-β family receptors directly. We captured type I receptors ALK2, ALK3, and ALK4, or type II receptors ActRIIA, ActRIIB, BMPRII, and TβRII on a sensor chip, as these receptors interact with the cognate Cripto-1/Cryptic ligands Nodal, BMP-4, and Activin B (50). We injected 6 μM Fc free Cripto-1 or Cryptic (Fig. 3*A*). Cripto-1 elicited a strong SPR response when injected over ALK4. But the response was dominated by extremely fast on- and off-rates, indicating it is dominated by significant bulk shift or nonspecific binding components (Fig. 3*A*). A weaker response with similarly fast kinetics could also be observed with other receptors. In contrast to Cripto-1, Cryptic did not elicit an SPR response with any captured receptors (data not shown).

To identify the source of the SPR response, we evaluated the Cripto-1-ALK4 dose-response relationship. We titrated Fc free Cripto-1 over ALK4 at concentrations ranging from 46 nM to 24 μM (Fig. 3*B*). As anticipated from our single injection studies, the SPR response increased with Cripto-1 concentrations. But the SPR response did not follow Langmuir adsorption kinetics (Fig. 3*B*). Thus, we fit our binding data using a "one-site total binding" model and obtained a K_d of ~750 nM with a maximum specific binding value (B_{max}) of 62.5 response units (RU) (Fig. 3*B*) (51). Based on this analysis and the observation that Cripto-1 caused small SPR responses with other tested receptors (Fig. 3*A*), we propose that the Cripto-1-ALK4 interaction is weak, and that Cripto-1 can interact nonspecifically with receptors. Notably, when we injected ALK4 over captured Cripto-1, we observed a similar response dominated by bulk shift and kinetic rate constants (data not shown).

Earlier studies indicated the CFC domain interacts directly with ALK4 (52). To assess this observation, we captured domain deletion constructs on a sensor chip and injected 24 μM ALK4. We hypothesized that constructs, which include the CFC domain, bind ALK4, but constructs that lack the CFC

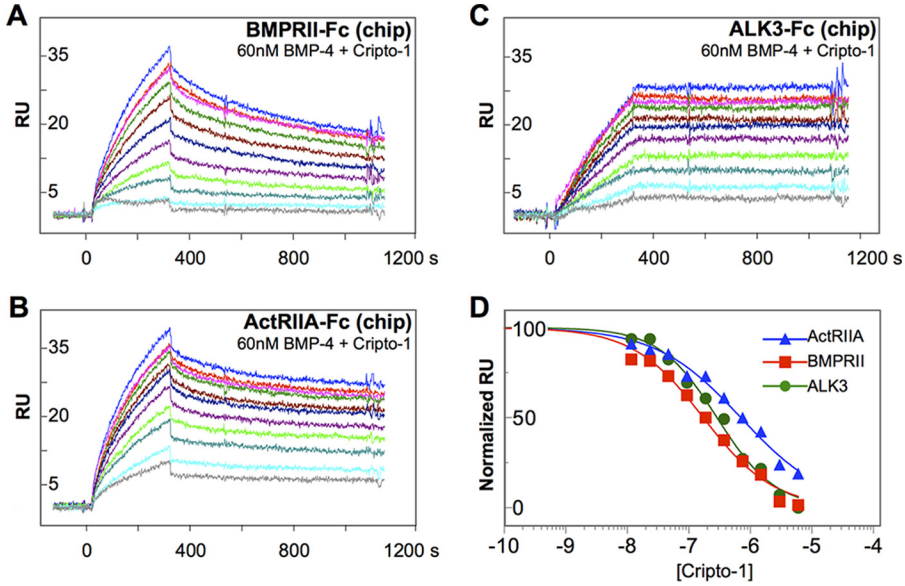

FIGURE 4. **Mapping the Cripto-1-ligand interaction.** BMPRII-Fc (*A*), ActRIIA-Fc (*B*), and ALK3-Fc (*C*) were captured on the sensor chip. 60 nM BMP-4 was preincubated with 0 (*blue*), 11.72 (*red*), 23.44 (*magenta*), 46.88 (*dark green*), 93.75 (*maroon*), 187.5 (*dark blue*), 375.0 (*purple*), 750.0 (*bright green*), 1500.0 (*teal*), 3000.0 (*cyan*), and 6000.0 nM (*gray*) Fc free Cripto-1. Cripto-1-BMP-4 mixtures were injected over the sensor chip. *D*, IC_{50} determination. Raw RU values at 150 s post-injection were taken for each Cripto-1 concentration. RU values were normalized and fitted using the non-linear regression algorithm implemented in GraphPad. S.E. are small and were omitted for clarity (37).

domain do not. As anticipated, we observed an SPR response with all CFC domain constructs, but not with constructs lacking this domain (Fig. 3*C*). However, responses were again dominated by bulk shift, indicating the interaction is weak and has significant nonspecific elements. To obtain an independent measure of Cripto-1·ALK4 binding, we used glutaraldehyde cross-linking and SDS-PAGE. We hypothesized that a cross-linking product would show Cripto-1·ALK4 complexes are stable. But we failed to detect adducts using this approach (Fig. 3*D*).

To determine whether ligands help stabilize Cripto-1·ALK4 or other Cripto-1·receptor complexes, we performed two independent SPR experiments. First, we captured ALK4-Fc, ActRIIA-Fc, or ActRIIB-Fc on the sensor chip and injected Nodal or Nodal preincubated with Fc-free Cripto-1 (Fig. 3*E*). Strikingly, whereas Cripto-1 did not have a noticeable effect on the weak Nodal-ALK4 interaction, indicating Cripto-1 does not stabilize Nodal·ALK4 complexes in this format (Fig. 3*E*), Cripto-1 prevented binding of Nodal to the type II receptors ActRIIA and ActRIIB. In a second experiment, we captured Cripto-1-Fc and injected Nodal alone or Nodal preincubated with ALK4 (Fig. 3*F*). ALK4 did not enhance Cripto-1·Nodal complexation. We therefore conclude that Cripto-1·ALK4 complexes are weak and that a direct interaction between these two proteins may not be very consequential.

Cripto-1 and Cryptic Block Ligand Association with Type II and Some Type I Receptors—It is well established that Cripto-1 and Cryptic interact with TGF-β family ligands (9, 26, 33, 34), but how they bind ligands is not clear. Based on molecular knowledge about the TGF-β family ligand-receptor interaction (38), we hypothesized Cripto-1 and Cryptic either contact ligand surfaces that overlap with receptor binding sites (and thus compete with receptors for ligand binding), or they contact ligand surfaces that do not overlap with receptor binding sites (and thus form multimeric complexes with ligands and receptors, as is suggested). To test this hypothesis, we used an SPR-based co-binding/inhibition assay (37). In this format, receptor-Fc fusion constructs were captured on the sensor chip and a constant concentration of ligand preincubated with increasing concentrations of Cripto-1 or Cryptic was injected. If Cripto1/Cryptic and receptors occupy the same ligand surface, the SPR signal is expected to decrease with increasing Cripto-1/Cryptic concentrations. But, if Cripto1/Cryptic and receptors occupy different ligand surfaces, the SPR signal is expected to increase with increasing Cripto-1/Cryptic concentrations (37).

Using this approach, we discovered that soluble Cripto-1 prevents BMP-4 binding to type I receptor ALK3 and type II receptors ActRIIA and BMPRII in a concentration-dependent manner (Fig. 4, *A*–*C*), replicating our observation with Nodal (Fig. 3*E*). The reaction followed a sigmoidal inhibition curve (Fig. 4*D*), indicating Cripto-1 competitively inhibited BMP-4 binding to its receptors. Based on the changing SPR response (37), we calculated IC_{50} values for inhibition of BMP-4 binding to ActRIIA (705 nM), BMPRII (173 nM), and ALK3 (288 nM) (Table 2). Soluble Cryptic showed a similar behavior (Fig. 5, *A* and *B*). But the effect of Cryptic on Activin B was more discriminatory, as Cryptic-Fc blocked Activin B binding to the type II receptor BMPRII much more effectively than to ActRIIA (Fig. 5*C*). We calculated IC_{50} values for inhibition of Activin B binding to BMPRII (288 nM) and ActRIIA (1024 nM) (Table 2). We did not investigate the function of Cryptic in the Activin B-type I receptor interaction, as high affinity type I receptors for Activin B are not known. Significantly, Cripto-1 also prevented Nodal binding to type II receptors (Fig. 3*E*), but these findings are preliminary, as the activity of currently available Nodal is not consistent. Even so, our studies support the conclusion that Cripto-1 and Cryptic contact ligands at or near their type I and type II receptor binding sites.

TABLE 2
SPR-based half-maximal inhibitory concentrations (IC_{50})

SPR binding		Chip		
Analyte	Inhibitor[a]	ActRIIA-Fc	BMPRII-Fc	ALK3-Fc
	nM			
BMP-4	Cripto-1	705.1 ± 74.5	172.9 ± 19.0	288.8 ± 28.5
Activin B	mCryptic	1024 ± 60.9	288.2 ± 14.5	

[a] 10 concentrations of inhibitor were used.

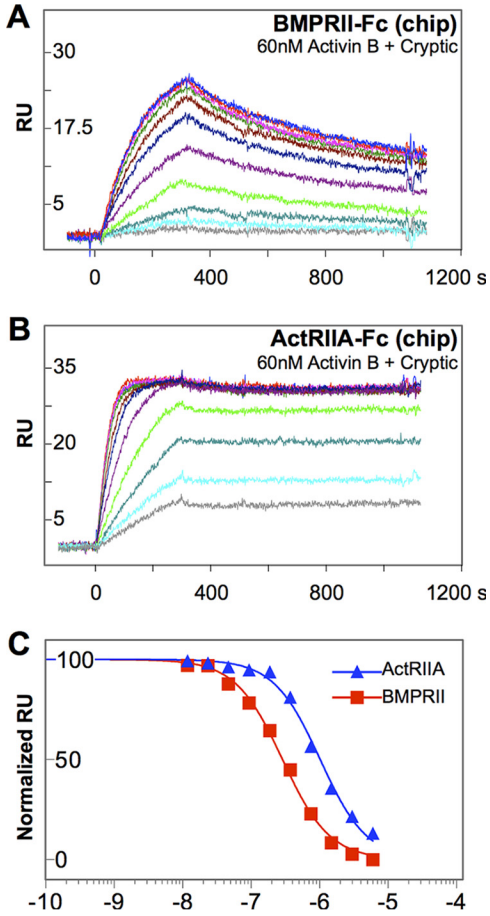

FIGURE 5. **Mapping the Cryptic-ligand interaction.** BMPRII-Fc (*A*) and ActRIIA-Fc (*B*) were captured on the sensor chip. 10 nM Activin B was preincubated with 0 nM (*blue*), 11.72 (*red*), 23.44 (*magenta*), 46.88 (*dark green*), 93.75 (*maroon*), 187.5 (*dark blue*), 375.0 (*purple*), 750.0 (*bright green*), 1500.0 (*teal*), 3000.0 (*cyan*), and 6000.0 nM (*gray*) Fc-free Cryptic. Activin B-Cryptic mixtures were injected over the sensor chip. *C*, IC_{50} determination. Raw RU values from SPR measurements were taken for each Cryptic concentration at 150 s post-injection. RU values were normalized and fitted using the non-linear regression algorithm implemented in GraphPad. S.E. are small and were omitted for clarity (37).

Soluble Cripto-1 and Cryptic Inhibit Signaling—As Cripto-1 and Cryptic inhibited ligand-receptor binding, we hypothesized they could also inhibit ligand signaling. To test this hypothesis, we used reporter gene expression assays. We transfected HepG2 hepatocellular carcinoma cells with control plasmid pGL4.74 (hRluc) and the SMAD-3 responsive reporter plasmid pGL4.48 (luc2P/SBE) or the SMAD-1/5/8 responsive reporter plasmid pGL3 (luc2P/BRE) (Fig. 6) (53, 54). We treated transfected cells with 1 nM BMP-4 or Activin B and increasing concentrations of Cripto-1-Fc or Cryptic-Fc (0–5000 nM). Both ligands induced luciferase reporter activity and both Cripto-1-Fc and Cryptic-Fc reduced the luciferase signal in a concentration-dependent manner. Cripto-1-Fc abrogated the BMP-4-mediated SMAD-1/5/8 response completely (Fig. 6*A*, Table 3). Cryptic-Fc exhibited an intriguing behavior. It blocked Activin B-mediated SMAD-1/5/8 signaling completely. But inhibition followed a biphasic dose-response (Fig. 6*C*), indicating it blocks at least two distinct Activin B signaling complexes with different potency. Notably, Cryptic-Fc inhibited the Activin B-induced SMAD-2/3 signal only by about half (Fig. 6*D*), indicating signaling may be activated differentially by type II receptors. As indicated by our SPR data (Fig. 5), Cryptic-Fc may block activation by one receptor (BMPRII) much more effectively than by others (ActRIIA, ActRIIB).

To validate Cripto-1 domain functions, we also evaluated their inhibitory potency (Fig. 6*B*). We treated transfected HepG2 cells with 1 nM BMP-4 and 1000 nM Cripto-1-Fc domain constructs. Matching our SPR results (Fig. 2*G*), only full-length Cripto-1-Fc (NEC-Fc) exhibited full inhibitory potency (a 5-fold reduction in signaling from 30 to 6 *Renilla* luciferase units (RLU)). Both two-domain constructs (NE-Fc and EC-Fc) showed residual inhibitory activity, but were far weaker than the full-length construct. They reduced signaling only from 30 to about 20 RLU. Single domains (E-Fc and C-Fc) did not inhibit signaling.

Membrane-associated Cripto-1 Potentiates BMP-4 Signaling—Endogenously expressed, membrane-anchored Cripto-1 is known for its ability to potentiate Nodal signaling (26, 30, 46, 47). By contrast, we discovered that soluble Cripto-1-Fc inhibits Nodal and BMP-4 signaling (Figs. 4–6). To reconcile these two opposing activities we examined how endogenously expressed and overexpressed Cripto-1 affect BMP-4 signaling (Fig. 7). We found that Cripto-1 was efficiently overexpressed in transiently transfected HepG2 cells (Fig. 7, *A* and *B*) and strongly knocked down by shRNA in endogenously expressing NT2/D1 cells (Fig. 7*C*). Consistent with the potentiating activity of membrane-anchored Cripto-1, BMP-4 signaling was 2–3-fold higher in HepG2 cells transfected with Cripto-1 expression vector compared with HepG2 cells transfected with control vector (Fig. 7*D*). But Cripto-1 did not potentiate signaling by the BMP-4 homolog BMP-2, which we found does not bind Cripto-1 (Fig. 2*A*). In agreement with our earlier findings, soluble Cripto-1-Fc neutralized the potentiating activity of membrane-associated Cripto-1 in HepG2 cells (Fig. 7*E*), revealing key functional differences between soluble and membrane-bound forms. In support of our findings using HepG2 cells and Cripto-1 overexpression, BMP-4 signaled effectively in NT2/D1 cells transfected with scrambled shRNA vector, whereas Cripto-1 shRNA knockdown strongly suppressed BMP-4 signaling activities (Fig. 7*F*). Taken together, our findings indicate that membrane-anchored Cripto-1 can potentiate signaling by its cognate ligands, whereas the soluble form can inhibit signaling and outweigh the activities of the membrane-anchored form.

Soluble Cripto-1 Prevents BMP-4-dependent XEN Cell Differentiation—BMP-4 is a key regulator of embryogenesis that promotes differentiation of multipotent XEN cells to extraembryonic visceral endoderm (VE) identity (39, 40). We hypothesized, if soluble Cripto-1 inhibits BMP-4 signaling, it will interfere with BMP-4-mediated XEN cell differentiation.

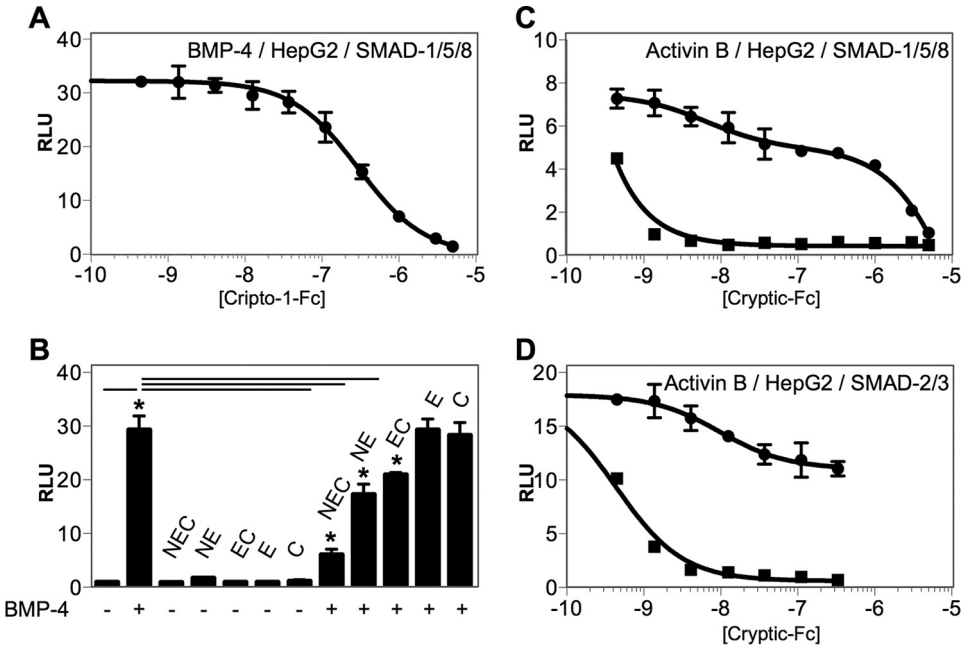

FIGURE 6. **Signaling inhibition by soluble Cripto-1 and Cryptic.** *A,* Cripto-1-Fc suppresses BMP-4 signaling. BMP-4 (1 nM) induces expression of a SMAD-1/5/8-responsive luciferase reporter. Cripto-1-Fc inhibits the BMP-4-dependent luciferase signal in a concentration-dependent manner. The *y* axis shows RLU. The *x* axis shows Cripto-1 concentration in log scale (*M*). *B,* individual Cripto-1 domains lack inhibitory potency. BMP-4 (1 nM) induces expression of a SMAD-1/5/8-responsive luciferase reporter. Full-length Cripto-1-Fc (*NEC*) almost completely inhibits BMP-4 signaling, Cripto-1 constructs that comprise two domains (*NE* and *EC*) reduce BMP-4 signaling but are much less potent than the full-length (*NEC*) form. Single domain constructs (*E* and *C*) do not inhibit BMP-4 signaling. Statistically significant differences are marked by an *asterisk* and are linked to the comparison value by a *black bar*. *C* and *D*, Cryptic-Fc suppresses Activin B signaling. 1 nM Activin B induces expression of both SMAD-2/3 (*C*) and SMAD-1/5/8 (*D*) responsive luciferase reporters. Cryptic-Fc (*circles*) inhibits the Activin B-dependent luciferase signal in a concentration-dependent manner. Inhibition follows a biphasic curve and inhibits SMAD-1/5/8 pathways more effectively than SMAD-2/3 pathways. S.E. of biphasic curve-fitting are not calculated. For comparison, inhibition of Activin B signaling by ActRIIA-Fc (*squares*) is also shown. The *y* axis shows RLU. The *x* axis shows the Cryptic-Fc concentration in log scale (*M*). All values are shown as average of 4 biological replicates. *Error bars* correspond to S.E. Errors from ActRIIA-Fc inhibition are less than 5% and thus are not shown.

TABLE 3

Cell-based half-maximal inhibitory concentrations (IC_{50})

The reporter gene expression study was performed in quadruplicate.

Ligand	Reporter	Inhibitor[a]	IC_{50} 1st phase	IC_{50} 2nd phase
			*n*M	
BMP-4	SMAD-1/5/8	Cripto-1-Fc	207.1 ± 34.3	
Activin B	SMAD-1/5/8	mCryptic-Fc	6.400	13,061.7
Activin B	SMAD-2	mCryptic-Fc	ND[b]	ND
Activin B	SMAD-1/5/8	ActRIIA-Fc	0.4220 ± 0.011	
Activin B	SMAD-2	ActRIIA-Fc	0.5100 ± 0.035	

[a] 10 concentrations of inhibitor were used.
[b] ND, not determined.

To test this hypothesis, we examined morphological and gene expression changes of XEN cells cultured in the presence or absence of BMP-4, or BMP-4 and Cripto-1-Fc. As expected, BMP-4 promoted a profound morphological change in XEN cells, reminiscent of the epithelial VE (Fig. 8*A*, compare untreated with BMP-4-treated panels). In addition, expression of VE markers was strongly induced (Fig. 8*B*). However, co-culture with Cripto-1-Fc strongly suppressed both morphological and gene expression changes normally induced by BMP-4 (Fig. 8, *A*, compare *BMP-4* and *BMP-4* + *Cripto-1*, and *B*), indicating that soluble Cripto-1-Fc can interfere with BMP-4-induced differentiation of XEN cells, and thus act as a BMP-4 antagonist in a stem cell model of development.

Discussion

The EGF-CFC family proteins Cripto-1 and Cryptic are essential regulators of TGF-β family signaling (2). They appear to have dual functions: as co-receptors of Nodal-related ligands (3, 30, 31), and as antagonists of Activins and TGF-βs (28, 34–36). To reconcile these dichotomous activities, we aimed to elucidate their mechanism of action. Using recombinant human Cripto-1 and mouse Cryptic, we discovered both molecules interact with a limited number of TGF-β family ligands. Cripto-1 interacted with Nodal and BMP-4, Cryptic interacted with Activin B. Intriguingly, a recent study found that Cripto-1 is expressed at the bottom of colonic crypts in normal human and mouse colon (55), indicating it could regulate signaling of BMP-4 expressed by intravillus and intercrypt mesenchymal cells that are adjacent to intestinal stem cells (56). It has been suggested that Cripto-1 and Cryptic have similar, possibly redundant functions. But our biophysical evidence indicates there are clear functional differences between the two molecules. Thus, we propose Cripto-1 and Cryptic have distinct, non-overlapping ligand binding and regulatory functions.

Previous studies have indicated that Cripto-1 binds the TGF-β family receptor ALK4. This interaction is thought to be critical for Cripto-1 co-receptor function and Nodal signaling (26, 28, 47). To evaluate its functional significance, we investigated whether Cripto-1 or Cryptic bind ALK4 or other TGF-β family receptors directly. Using SPR, we detected a response when probing Cripto-1 binding to ALK4. However, although these results appear to confirm an interaction, they are not conclusive, as the response is dominated by a nonspecific binding component. Significantly, Cripto-1 did not cross-link with ALK4 in solution or improve Nodal·ALK4 complexation. We

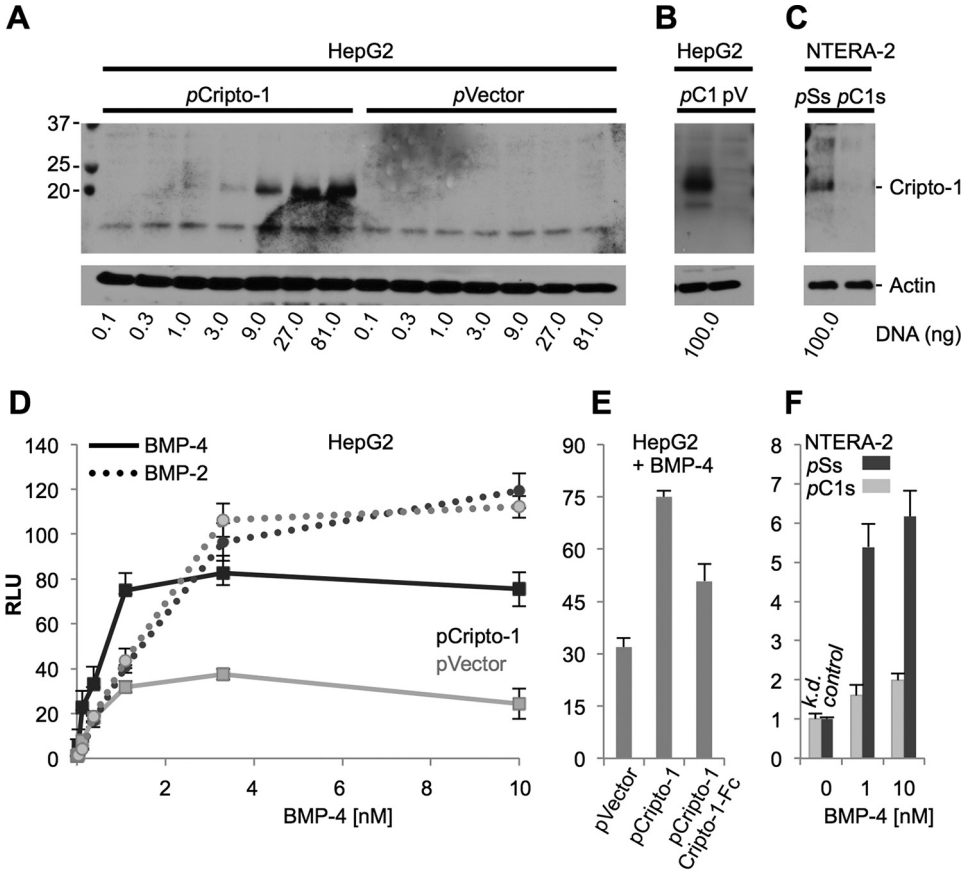

FIGURE 7. **Signal-potentiating activities of membrane-associated Cripto-1.** *A,* Western blot of Cripto-1 overexpression in HepG2 cells. Cells were transfected with a control (*p*Vector) or Cripto-1 (*p*Cripto-1) expression vector at the indicated concentrations. Expression of membrane-associated (GPI-anchored) Cripto-1 was detected using the monoclonal anti-Cripto-1 antibody ab108391. *B,* Western blot of Cripto-1 overexpression in HepG2 cells as used for reporter assay (*D* and *E*). Cells were transfected with 100 ng of control (*p*V) or Cripto-1 (*p*C1) expression vector. *C,* Western blot of Cripto-1 knockdown in NT2/D1 cells as used for the reporter assay (*F*). Cells were transfected with 100 ng of scrambled (*p*Ss) or Cripto-1 (*p*C1s) shRNA vector. *D*, comparison of BMP-4 signaling (*squares*, *solid lines*) and BMP-2 signaling (*circles*, *dotted lines*) in HepG2 cells transfected with Cripto-1 expression vector (*dark shade*) or control vector (*light shade*). Signaling was induced with increasing concentrations of BMP-4 or BMP-2 as shown. Membrane-bound Cripto-1 potentiates BMP-4 but not BMP-2 signaling. *E*, inhibition of signal potentiation with soluble Cripto-1. HepG2 cells transfected with control (*p*Vector) or Cripto-1 (*p*Cripto-1) expression vector were treated with 1 nM BMP-4 or 1 nM BMP-4 and 500 nM Cripto-1-Fc. Soluble Cripto-1-Fc inhibits BMP-4 signaling even with co-expression of membrane-bound Cripto-1. *F,* signal potentiation in Cripto-1 expressing NT2/D1 cells. Cells were transfected with 100 ng of Cripto-1 shRNA vector (*sC-1*, *light gray bars*) or scrambled shRNA vector (*sSc*, *dark gray bars*). Cells were treated with 1 or 10 nM BMP-4. Cripto-1 knockdown (*light gray bars*) reduces BMP-4 signaling relative to the scrambled shRNA control (*dark gray bars*). Data are expressed as mean ± S.E. of four biological replicates. Of note, previous studies have demonstrated that the magnitude of the luciferase signal is cell line dependent (50).

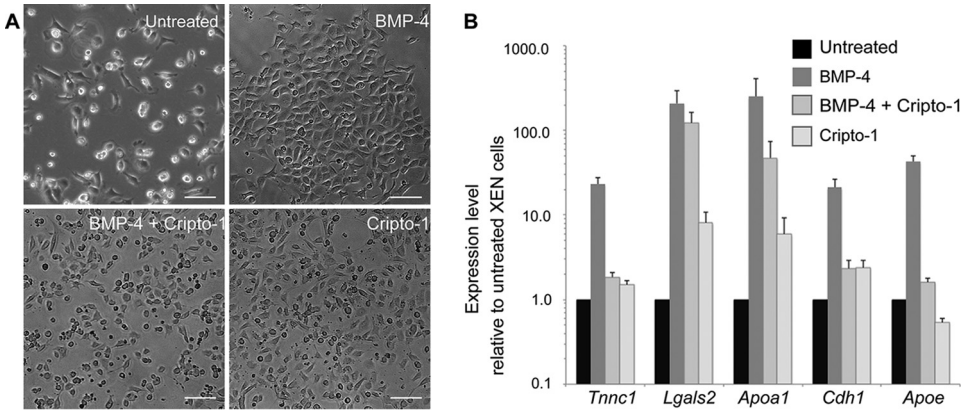

FIGURE 8. **XEN cell differentiation.** *A,* cell morphologies of XEN cells cultured in stem cell self-renewal conditions, which causes cells to grow as single cells (untreated), or in the presence of 50 ng/ml of BMP-4, which causes cells to epithelialize (*top right*). By contrast, 50 μg/ml of Cripto-1 (*bottom left*) interferes with BMP-4-induced epithelialization, whereas Cripto-1 alone (50 μg/ml) induces minimal changes on XEN cell morphology (*bar* = 100 μm). *B,* quantitative real-time PCR analysis of differentiated VE gene expression in XEN cells cultured in stem cell self-renewal conditions (untreated, *black*), BMP-4 treated (*dark gray*), BMP-4 + Cripto-1 treated (*medium gray*), and Cripto-1 treated (*light*), indicating that Cripto-1 strongly suppresses BMP-4-induced expression of VE gene expression.

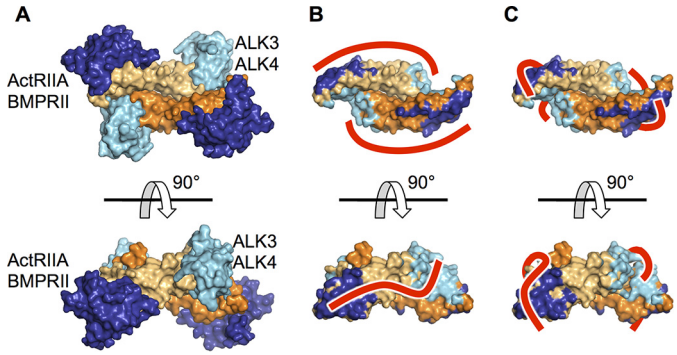

FIGURE 9. **Molecular basis of ligand binding.** *A,* ligand-receptor complex based on the BMP-9-ALK1-ActRIIB structure (59). The disulfide-linked homodimeric ligand (center, *orange*) binds the extracellular domains of type I Activin receptor-like kinases (*light blue*) and type II Activin and BMP receptors (*dark blue*). Cripto-1 prevents ligand binding to type I and type II receptors indicating it contacts the receptor interaction surfaces on ligands. *B,* ipsilateral binding model. Receptor binding surfaces on the homodimeric ligand (*orange*) are shown. *Light blue* surfaces contact type I receptors, *dark blue* surfaces contact type II receptors. In this binding model, a Cripto-1/Cryptic protomer contacts one side of the dimeric ligand. *C,* contralateral binding model. Receptor binding surfaces on the ligand are shown. *Light blue* surfaces contact type I receptors, *dark blue* surfaces contact type II receptors. In this model, a Cripto-1/Cryptic protomer contacts both interaction surfaces of one ligand protomer.

therefore conclude that the direct interaction between soluble Cripto-1 and ALK4 is weak, possibly nonspecific and of limited consequence. However, our findings do not exclude a role for Cripto-1 in ALK4-dependent Nodal signaling. Previously, this interaction was investigated by co-immunoprecipitation (9, 26). These studies showed Cripto-1 co-precipitated with ALK4. It is possible that the cell-based approach masked a more complex behavior. Namely, Cripto-1·ALK4 complexes could have been bridged by ligands that are present in the cell-growth medium. Alternatively, cell-surface proteins like LRP5, LRP6, or glypican could have facilitated Cripto-1·ALK4 complexation (57, 58). Or ALK4 could have contacted the GPI linker, which is not present in Fc fusion forms. Although we show that the direct Cripto-1·ALK4 ectodomain interaction is weak and possibly nonspecific, whether Cripto-1 interacts with ALK4 indirectly, and what the function of this complex is, remains to be determined.

The most widely recognized function of Cripto-1 is as Nodal co-receptor (2). It is suggested Cripto-1 binds Nodal and potentiates Nodal signaling by stabilizing Nodal·ALK4 complexes (9, 23, 25, 26, 30). But Cripto-1 also antagonizes Activin and TGF-β signaling (28, 35, 36). To reconcile these divergent functions, we investigated how Cripto-1 and Cryptic recognize ligands. We speculated that molecular knowledge of this interaction could help clarify their biological functions. Using an SPR-based approach that enables binding site mapping (37), we discovered Cripto-1 and Cryptic contact ligand surfaces that are also recognized by type I or type II receptors (Fig. 9). Although unexpected, these findings are not surprising, as ligands are small, and a large fraction of their surface is covered by receptors when they form signaling complexes (38, 59). As our findings indicated there is significant overlap between the Cripto-1, Cryptic, and receptor binding sites on ligands, we hypothesized that soluble Cripto-1 and Cryptic could function as inhibitors of their cognate ligands *in vitro*. As predicted, Cripto-1-Fc inhibited BMP-4-dependent reporter gene expression and differentiation of XEN cells to VE, consistent with the observation that VE formation is aberrant in Cripto-1 knockout embryos (8).

By contrast, Cryptic-Fc inhibited Activin B-dependent reporter gene expression, supporting the conclusion that Cripto-1 and Cryptic have differing activities. Strikingly, the Cryptic-Fc reaction revealed a biphasic dose-response. As Cryptic-Fc was a far more effective inhibitor of Activin B-BMPRII than Activin B-ActRIIA binding, we propose the biphasic response reflects differential inhibition of BMPRII and ActRIIA signaling complexes *in vitro*.

Taken together, our biophysical and *in vitro* studies show Cripto-1 and Cryptic can compete with receptors for ligand binding, thus revealing the molecular basis of their interaction with ligands. As Cripto-1 and Cryptic appear to bind ligands at or near receptor binding sites (Fig. 9), it is not surprising that the soluble Fc-fusion forms effectively inhibit signaling by their cognate ligands. But our findings raise critical questions about the co-receptor function. How can Cripto-1 or Cryptic potentiate signaling when their soluble forms prevent ligand-receptor complex formation? We propose that this mechanism has precedent in the repulsive guidance molecule (RGM) family of GPI anchored co-receptors (60–62). Like Cripto-1 and Cryptic, membrane-anchored RGMs potentiate BMP signaling, whereas their soluble forms inhibit BMP signaling (63). Recent crystal structures explain the inhibitory function of RGMs. Similar to Cripto-1 and Cryptic, they occupy type I receptor binding sites on ligands and thus inhibit signaling (64). To reconcile the RGM co-receptor and inhibitor functions, the authors propose RGMs help target BMP ligands into endosomes (64), which are enriched with TGF-β family receptors (65). Thus, RGMs could help potentiate signaling. We propose Cripto-1 and Cryptic could have similar trafficking functions, which are mediated by GPI-dependent membrane attachment and endosomal membrane localization (42). Indeed, overexpression of GPI-anchored Cripto-1 on the cell surface potentiates BMP-4 signaling, whereas knockdown of endogenously expressed Cripto-1 reduces BMP-4 signaling, revealing a distinct, but critical function of the membrane-associated forms. We propose Cripto-1 and Cryptic may provide a mechanism for ligand capture at the cell surface and help target cognate ligands into receptor-rich endosomes for signal potentiation.

In conclusion, we have elucidated the molecular basis of ligand recognition by the EGF-CFC family co-receptors Cripto-1 and Cryptic. Our findings reveal an unexpected molecular function that may be paralleled by the RGM family of GPI-anchored co-receptors. Namely, like RGMs, Cripto-1 and Cryptic contact receptor interaction surfaces on TGF-β family ligands. Thus, their soluble forms can function as inhibitors of ligand-receptor binding. But our findings also raise many new questions. Does the inhibitor function have a biological role? Do endocytosis or trafficking explain how membrane-anchored Cripto-1 and Cryptic potentiate signaling (41, 42)? Can the co-receptor and inhibitor functions be reconciled?

Materials and Methods

TGF-β Family Ligands—Activin A (338-AC/CF), Activin B (659-AB/CF), and TGF-β1 (240-B/CF) were purchased from R&D Systems or produced in house. Nodal (3218-ND/CF), GDF-1 (6937-GD/CF), GDF-3 (958-G3/CF), GDF-8 (788-G8/CF), GDF-11 (1958-GD/CF), GDF-15 (957-GD/CF), BMP-4 (314-BP/CF), and BMP-9 (3209-BP/CF) were purchased from R&D Systems. BMP-2 (C-67309), BMP-6 (C-67307), BMP-7 (C-67319), BMP-10 (C-67317), TGF-β2 (C-63498), and TGF-β3 (C-63508) were purchased from PROMOCELL. We note that both BMP-4 and GDF-3 lose activity within 8 weeks after reconstitution under the recommended conditions.

Expression Plasmids—Synthetic *Cripto-1-hIgg-Fc* and *cryptic-hIgg-Fc* genes were obtained from GeneArt. Full-length fusion constructs included the human Cryptic signal peptide (1–25), and the extracellular domains of human Cripto-1(31–163) and mouse Cryptic(36–175). Functional domains were linked to human IgG1 Fc via a 22-amino acid long linker containing a tobacco etch virus cleavage site, a glycine/serine-rich region, and a FLAG tag. Domain deletion constructs were generated by PCR or were purchased from GeneArt.

Protein Purification—Proteins were expressed using stably transfected Chinese hamster ovary cell pools. The secreted fusion constructs were captured from conditioned medium using Protein A affinity chromatography, eluted with 100 mM glycine, pH 3.0, subjected to SEC, dialyzed into phosphate-buffered saline, pH 7.5, and stored at −20 or −80 °C. For inhibition assays, the Fc was removed using tobacco etch virus protease followed by protein A affinity chromatography and SEC. Purity was determined with SDS-PAGE.

Cell Lines—CHO cells were obtained from Life Technologies. HepG2 cells (HB-8065) and NTERA2 cl.D1 (NT2/D1) cells (CRL-1973) were obtained from ATCC (American Type Culture Collection) and maintained as indicated by the supplier. Briefly, HepG2 and NT2/D1 cells were grown in Eagle's minimum essential medium supplemented with 10% FBS and 1% penicillin/streptomycin at 37 °C in 5% CO_2 and 10% CO_2, respectively. Cells were passaged at least three times before performing assays. Passage number did not exceed 15. XEN cell lines were cultured as described (66).

Surface Plasmon Resonance—Binding affinities and inhibition were determined using the Biacore 2000. Anti-human IgG (Fc) antibody was immobilized onto four channels of a CM5 chip using amine coupling chemistry. 200–300 RU of purified Cripto-1-Fc, Cryptic-Fc, ActRIIA-Fc, ActRIIB-Fc, BMPRII-Fc, ALK3-Fc, or ALK4-Fc were captured on the experimental channels. A reference channel was monitored to account for nonspecific binding, drift, and bulk shifts. To determine ligand-binding specificity, 80 nM of each ligand (see ligands above) was injected over captured Cripto-1 or Cryptic. For analysis of Cripto-1/Cryptic binding to receptors, Fc-free forms at concentrations up to 24 μM were injected over captured receptors. For ligand binding kinetics, a concentration series of interacting ligands (BMP-4, Activin B, or GDF-3) was injected over captured Cripto-1 or Cryptic. To determine whether Fc dimerization causes differences in ligand binding, 4000 RU of Cripto-1 was cross-linked on the experimental channel and a concentration series of BMP-4 was injected over immobilized Cripto-1. For inhibition analysis, BMP-4 or Activin B at one concentration preincubated with various concentrations of Fc-free Cripto-1 or Cryptic was injected over captured receptors. To determine whether the presence of a ligand affects the interaction between Cripto-1 and receptors, BMP-4 or Nodal at one concentration were preincubated with Fc-free Cripto-1 or Alk4 and injected over captured receptors. For deglycosylation experiments, Cripto-1 constructs were treated with PNGase F and Sialidase and captured on the sensor chip. SDS-PAGE was used to evaluate the glycosylation status. Deglycosylation enzymes were removed using a metal affinity column. All experiments were carried out at 25 °C. HBS-EPS buffer (0.01 M HEPES, 0.5 M NaCl, 3 mM EDTA, 0.005% (v/v) Tween 20, pH 7.4) containing 0.1% BSA (Sigma) was used as running buffer at a flow rate of 50 μl/min. Nodal containing samples were kept without BSA, as it causes rapid inactivation. After each binding cycle, the antibody surface was regenerated to baseline. Sensorgrams were analyzed by double referencing. To obtain kinetic rate constants, the processed data were fitted to 1:1 "two-state reaction model" using BiaEvaluation software. The equilibrium binding constant K_d was determined by calculating the ratio of binding rate constants k_d/k_a. Results are summarized in Table 1. For Cripto-1·ALK4 binding we used Biaevaluation and GraphPad Prism version 6.0h. We obtained best-fit curves by nonlinear curve fitting using a "one-site total binding" model. We determined B_{max}, K_d, and nonspecific (NS) binding contributions. For competition experiments, we obtained a best-fit inhibition curve using a non-linear regression algorithm for log(antagonist) *versus* normalized response model (37).

Cross-linking—Approximately 4 μg of protein samples were cross-linked with 0.01 or 0.02% glutaraldehyde for 20 min at room temperature. Native cross-linking reactions were performed in PBS. The cross-linking reaction was quenched with Tris buffer at pH 8 (final concentration: 200 mM). Samples were analyzed by 12% SDS-PAGE under reducing conditions.

Reporter Assays—For standard reporter assays, ~10,000 HepG2 cells/well in complete medium (Eagle's minimum essential medium (DMEM) supplemented with 10% FBS and 1% penicillin/streptomycin) were seeded in a 96-well plate and grown overnight. Each well was transfected with 0.25 μl of Lipofectamine 2000, 200 ng of the SMAD1/5/8 responsive reporter plasmid pGL3 (luc2P/BRE) or the SMAD3 responsive reporter plasmid pGL4.48 (luc2P/SBE), and 2 ng of the (Luc2P/hRluc/TK) vector (control luciferase reporter plasmid, Promega). Transfection medium was removed the following day, and replaced with assay medium (serum free DMEM + 0.01% BSA) containing BMP-4, Activin B, Cripto-1-Fc, Cryptic-Fc, and/or ActRIIA-Fc. Assay medium was preincubated at 37 °C for 1 h before adding to cells. For Cripto-1 overexpression studies, ~10,000 HepG2 cells/well were seeded in a 96-well plate and grown overnight. Each well was transfected with 0.4 μl of Lipofectamine 2000, 100 ng of human TDGF-1 natural ORF mammalian expression plasmid (Sino Biological, HG10908-UT), or 100 ng of empty pCMV control vector, 100 ng of the SMAD1/5/8 responsive reporter plasmid, and 1 ng of the control reporter plasmid. Transfection medium was removed the following day, and replaced with assay medium containing a

concentration series of BMP-4, BMP-2, and/or Cripto-1-Fc. Assay medium was preincubated at 37 °C for 1 h before adding to cells. For Cripto-1 knockdown assays, ~10,000 NT2/D1 cells in complete medium were seeded in each well of a 96-well plate and grown overnight. Each well was transfected with 0.3 μl of Lipofectamine 3000, 100 ng of TDGF1 shRNA (5′-CCGGACAGCACAGTAAGGAGCTAAACTCGAGTTTAGCTCCTTACTGTGCTGTTTTTT-3′) (Sigma, SHCLNG-NM-003212) or scrambled shRNA control vector, 100 ng of the SMAD1/5/8 responsive reporter plasmid, and 1 ng of the control reporter plasmid. Transfection medium was removed the following day, and replaced with assay medium. After 48 h, assay medium was replaced with fresh assay medium containing 0, 1, and 10 nM BMP-4.

After addition of assay medium, cells were incubated for 16 h at 37 °C, luciferase activity was detected using a homemade dual-glow luciferase assay (44). Luminescence was determined using a FluoStar Omega plate reader. Relative luciferase units were calculated by dividing firefly luciferase units with *Renilla* luciferase units. To obtain IC_{50} values, we used a non-linear regression algorithm for log(antagonist) *versus* normalized response model (GraphPad). Data are expressed as mean of four independent measurements. Error bars correspond to S.E. of four biological replicates.

Immunoblotting—Cell lysates were prepared in RIPA buffer as previously described (50). Protein concentration of total cell lysate was determined with the Bradford assay. 10 μg of cell lysate were loaded on 12% SDS-polyacrylamide gels under reducing conditions. Western blot analysis was performed with antibodies specific for Cripto-1 (Abcam, ab108391) and β-actin (Cell Signaling, 8H10D10). WesternBright Sirius HRP substrate was used for detection (Advansta, K-12043-D10). Western blots were visualized by exposing the membrane to autoradiography film.

XEN Cell Differentiation Assays—In vitro differentiation followed previously described protocols (39, 40, 66). Briefly, cell culture dishes were treated with poly-L-ornithine (Sigma) for 30 min at room temperature, followed by Laminin (Sigma) at a final concentration of 0.15 $\mu g/cm^2$. XEN cells were plated at a density of ~20,000 cells/well of a 24-well dish in N2B27 medium (50% DMEM/F-12 (Invitrogen) + 50% neural basal medium (Invitrogen) + N2 medium (Invitrogen, ×100) + B27 (Invitrogen, ×50) + penicillin/streptomycin (10,000 units each), β-mercaptoethanol (55 mM)), and cultured overnight at 37 °C and 5% CO_2. On days 2, 4, and 6, the culture medium was replaced with fresh N2B27, N2B27 + 50 ng/μl of BMP-4, N2B27 + 50 ng/μl of BMP-4 + 50 μg/ml of Cripto-1-Fc, or N2B27 + 50 μg/ml of Cripto-1-Fc. After 6 days, cells in each treatment were imaged and harvested for mRNA analysis. RNA was harvested with TRIzol (Invitrogen), and reverse transcribed using Qiagen QuantiTect Reverse Transcription Kit. The resulting cDNA was analyzed on a Lightcycler 480 (Roche Applied Science) as described (66, 67).

Statistics—Cell-based assays were performed in quadruplicates and were repeated at least two different times. Statistical significance was determined using a two-tailed *t* test. *p* values <0.05 were considered statistically significant.

Author Contributions—S. A., A. R., and E. M. H. designed the experiments; S. A. performed molecular biology, protein expression, protein purification, SPR studies, reporter assays, and Western blots; T. P. performed XEN cell assays and RT-PCR; K. Y. C. assisted with protein expression, protein purification, and Western blots; J. R. assisted with expression and purification; M. F. assisted with RT-PCR methods; S. A., T. P., A. R., and E. M. H. analyzed data; E. M. H. wrote the manuscript; and S. A., E. M. H., and A. R. revised the manuscript.

Acknowledgments—We thank Dr. Washington Mutatu and Dr. Stacy Hovde for construction of expression vectors, Wendi Ni for assistance with protein purification.

References

1. Ciccodicola, A., Dono, R., Obici, S., Simeone, A., Zollo, M., and Persico, M. G. (1989) Molecular characterization of a gene of the "EGF family" expressed in undifferentiated human NTERA2 teratocarcinoma cells. *EMBO J.* **8,** 1987–1991
2. Shen, M. M., and Schier, A. F. (2000) The EGF-CFC gene family in vertebrate development. *Trends Genet.* **16,** 303–309
3. Saloman, D. S., Bianco, C., Ebert, A. D., Khan, N. I., De Santis, M., Normanno, N., Wechselberger, C., Seno, M., Williams, K., Sanicola, M., Foley, S., Gullick, W. J., and Persico, G. (2000) The EGF-CFC family: novel epidermal growth factor-related proteins in development and cancer. *Endocr. Relat. Cancer* **7,** 199–226
4. Schier, A. F. (2003) Nodal signaling in vertebrate development. *Annu. Rev. Cell Dev. Biol.* **19,** 589–621
5. Minchiotti, G., Parisi, S., Liguori, G., Signore, M., Lania, G., Adamson, E. D., Lago, C. T., and Persico, M. G. (2000) Membrane-anchorage of Cripto protein by glycosylphosphatidylinositol and its distribution during early mouse development. *Mech. Dev.* **90,** 133–142
6. Watanabe, K., Hamada, S., Bianco, C., Mancino, M., Nagaoka, T., Gonzales, M., Bailly, V., Strizzi, L., and Salomon, D. S. (2007) Requirement of glycosylphosphatidylinositol anchor of Cripto-1 for trans activity as a Nodal co-receptor. *J. Biol. Chem.* **282,** 35772–35786
7. Xu, C., Liguori, G., Persico, M. G., and Adamson, E. D. (1999) Abrogation of the *Cripto* gene in mouse leads to failure of postgastrulation morphogenesis and lack of differentiation of cardiomyocytes. *Development* **126,** 483–494
8. Ding, J., Yang, L., Yan, Y. T., Chen, A., Desai, N., Wynshaw-Boris, A., and Shen, M. M. (1998) Cripto is required for correct orientation of the anterior-posterior axis in the mouse embryo. *Nature* **395,** 702–707
9. Gritsman, K., Zhang, J., Cheng, S., Heckscher, E., Talbot, W. S., and Schier, A. F. (1999) The EGF-CFC protein one-eyed pinhead is essential for Nodal signaling. *Cell* **97,** 121–132
10. Bhattacharya, B., Miura, T., Brandenberger, R., Mejido, J., Luo, Y., Yang, A. X., Joshi, B. H., Ginis, I., Thies, R. S., Amit, M., Lyons, I., Condie, B. G., Itskovitz-Eldor, J., Rao, M. S., and Puri, R. K. (2004) Gene expression in human embryonic stem cell lines: unique molecular signature. *Blood* **103,** 2956–2964
11. International Stem Cell Initative, Adewumi, O., Aflatoonian, B., Ahrlund-Richter, L., Amit, M., Andrews, P. W., Beighton, G., Bello, P. A., Benvenisty, N., Berry, L. S., Bevan, S., Blum, B., Brooking, J., Chen, K. G., Choo, A. B., *et al.* (2007) Characterization of human embryonic stem cell lines by the International Stem Cell Initiative. *Nat. Biotechnol.* **25,** 803–816
12. Shen, M. M., Wang, H., and Leder, P. (1997) A differential display strategy identifies Cryptic, a novel EGF-related gene expressed in the axial and lateral mesoderm during mouse gastrulation. *Development* **124,** 429–442
13. Yan, Y. T., Gritsman, K., Ding, J., Burdine, R. D., Corrales, J. D., Price, S. M., Talbot, W. S., Schier, A. F., and Shen, M. M. (1999) Conserved requirement for EGF-CFC genes in vertebrate left-right axis formation. *Genes Dev.* **13,** 2527–2537
14. Gaio, U., Schweickert, A., Fischer, A., Garratt, A. N., Müller, T., Ozcelik, C., Lankes, W., Strehle, M., Britsch, S., Blum, M., and Birchmeier, C.

(1999) A role of the cryptic gene in the correct establishment of the left-right axis. *Curr. Biol.* **9,** 1339–1342
15. Strizzi, L., Bianco, C., Normanno, N., and Salomon, D. (2005) Cripto-1: a multifunctional modulator during embryogenesis and oncogenesis. *Oncogene* **24,** 5731–5741
16. Cocciadiferro, L., Miceli, V., Kang, K. S., Polito, L. M., Trosko, J. E., and Carruba, G. (2009) Profiling cancer stem cells in androgen-responsive and refractory human prostate tumor cell lines. *Ann. N.Y. Acad. Sci.* **1155,** 257–262
17. Miyoshi, N., Ishii, H., Mimori, K., Sekimoto, M., Doki, Y., and Mori, M. (2010) TDGF1 is a novel predictive marker for metachronous metastasis of colorectal cancer. *Int. J. Oncol.* **36,** 563–568
18. Xu, C. H., Sheng, Z. H., Hu, H. D., Hao, K. K., Wang, Q. B., and Yu, L. K. (2014) Elevated expression of Cripto-1 correlates with poor prognosis in non-small cell lung cancer. *Tumour Biol.* **35,** 8673–8678
19. Bamford, R. N., Roessler, E., Burdine, R. D., Saplakoğlu, U., dela Cruz, J., Splitt, M., Goodship, J. A., Towbin, J., Bowers, P., Ferrero, G. B., Marino, B., Schier, A. F., Shen, M. M., Muenke, M., and Casey, B. (2000) Loss-of-function mutations in the EGF-CFC gene CFC1 are associated with human left-right laterality defects. *Nat. Genet.* **26,** 365–369
20. Goldmuntz, E., Bamford, R., Karkera, J. D., dela Cruz, J., Roessler, E., and Muenke, M. (2002) CFC1 mutations in patients with transposition of the great arteries and double-outlet right ventricle. *Am. J. Hum. Genet.* **70,** 776–780
21. Sutherland, M. J., and Ware, S. M. (2009) Disorders of left-right asymmetry: heterotaxy and situs inversus. *Am. J. Med. Genet. C Semin. Med. Genet.* **151C,** 307–317
22. Shen, M. M. (2007) Nodal signaling: developmental roles and regulation. *Development* **134,** 1023–1034
23. Kumar, A., Novoselov, V., Celeste, A. J., Wolfman, N. M., ten Dijke, P., and Kuehn, M. R. (2001) Nodal signaling uses activin and transforming growth factor-β receptor-regulated Smads. *J. Biol. Chem.* **276,** 656–661
24. Minchiotti, G., Manco, G., Parisi, S., Lago, C. T., Rosa, F., and Persico, M. G. (2001) Structure-function analysis of the EGF-CFC family member Cripto identifies residues essential for nodal signalling. *Development* **128,** 4501–4510
25. Reissmann, E., Jörnvall, H., Blokzijl, A., Andersson, O., Chang, C., Minchiotti, G., Persico, M. G., Ibáñez, C. F., and Brivanlou, A. H. (2001) The orphan receptor ALK7 and the Activin receptor ALK4 mediate signaling by Nodal proteins during vertebrate development. *Genes Dev.* **15,** 2010–2022
26. Yeo, C., and Whitman, M. (2001) Nodal signals to Smads through Cripto-dependent and Cripto-independent mechanisms. *Mol. Cell* **7,** 949–957
27. Chen, C., and Shen, M. M. (2004) Two modes by which Lefty proteins inhibit nodal signaling. *Curr. Biol.* **14,** 618–624
28. Kelber, J. A., Shani, G., Booker, E. C., Vale, W. W., and Gray, P. C. (2008) Cripto is a noncompetitive activin antagonist that forms analogous signaling complexes with activin and nodal. *J. Biol. Chem.* **283,** 4490–4500
29. Fuerer, C., Nostro, M. C., and Constam, D. B. (2014) Nodal.Gdf1 heterodimers with bound prodomains enable serum-independent Nodal signaling and endoderm differentiation. *J. Biol. Chem.* **289,** 17854–17871
30. Yan, Y. T., Liu, J. J., Luo, Y., E., C., Haltiwanger, R. S., Abate-Shen, C., and Shen, M. M. (2002) Dual roles of Cripto as a ligand and coreceptor in the Nodal signaling pathway. *Mol. Cell. Biol.* **22,** 4439–4449
31. Cheng, S. K., Olale, F., Bennett, J. T., Brivanlou, A. H., and Schier, A. F. (2003) EGF-CFC proteins are essential coreceptors for the TGF-β signals Vg1 and GDF1. *Genes Dev.* **17,** 31–36
32. Liguori, G. L., Borges, A. C., D'Andrea, D., Liguoro, A., Gonçalves, L., Salgueiro, A. M., Persico, M. G., and Belo, J. A. (2008) Cripto-independent Nodal signaling promotes positioning of the A-P axis in the early mouse embryo. *Dev. Biol.* **315,** 280–289
33. Aykul, S., Ni, W., Mutatu, W., and Martinez-Hackert, E. (2015) Human cerberus prevents Nodal-receptor binding, inhibits Nodal signaling, and suppresses Nodal-mediated phenotypes. *PLoS ONE* **10,** e0114954
34. Adkins, H. B., Bianco, C., Schiffer, S. G., Rayhorn, P., Zafari, M., Cheung, A. E., Orozco, O., Olson, D., De Luca, A., Chen, L. L., Miatkowski, K., Benjamin, C., Normanno, N., Williams, K. P., Jarpe, M., LePage, D., Salomon, D., and Sanicola, M. (2003) Antibody blockade of the Cripto CFC domain suppresses tumor cell growth *in vivo*. *J. Clin. Invest.* **112,** 575–587
35. Gray, P. C., Harrison, C. A., and Vale, W. (2003) Cripto forms a complex with activin and type II activin receptors and can block activin signaling. *Proc. Natl. Acad. Sci. U.S.A.* **100,** 5193–5198
36. Gray, P. C., Shani, G., Aung, K., Kelber, J., and Vale, W. (2006) Cripto binds transforming growth factor β (TGF-β) and inhibits TGF-β signaling. *Mol. Cell. Biol.* **26,** 9268–9278
37. Aykul, S., and Martinez-Hackert, E. (2016) Determination of half-maximal inhibitory concentration using biosensor-based protein interaction analysis. *Anal. Biochem.* **508,** 97–103
38. Hinck, A. P. (2012) Structural studies of the TGF-βs and their receptors: insights into evolution of the TGF-β superfamily. *FEBS Lett.* **586,** 1860–1870
39. Artus, J., Douvaras, P., Piliszek, A., Isern, J., Baron, M. H., and Hadjantonakis, A. K. (2012) BMP4 signaling directs primitive endoderm-derived XEN cells to an extraembryonic visceral endoderm identity. *Dev. Biol.* **361,** 245–262
40. Paca, A., Séguin, C. A., Clements, M., Ryczko, M., Rossant, J., Rodriguez, T. A., and Kunath, T. (2012) BMP signaling induces visceral endoderm differentiation of XEN cells and parietal endoderm. *Dev. Biol.* **361,** 90–102
41. Blanchet, M. H., Le Good, J. A., Mesnard, D., Oorschot, V., Baflast, S., Minchiotti, G., Klumperman, J., and Constam, D. B. (2008) Cripto recruits Furin and PACE4 and controls Nodal trafficking during proteolytic maturation. *EMBO J.* **27,** 2580–2591
42. Blanchet, M. H., Le Good, J. A., Oorschot, V., Baflast, S., Minchiotti, G., Klumperman, J., and Constam, D. B. (2008) Cripto localizes Nodal at the limiting membrane of early endosomes. *Sci. Signal.* **1,** ra13
43. Schiffer, S. G., Foley, S., Kaffashan, A., Hronowski, X., Zichittella, A. E., Yeo, C. Y., Miatkowski, K., Adkins, H. B., Damon, B., Whitman, M., Salomon, D., Sanicola, M., and Williams, K. P. (2001) Fucosylation of Cripto is required for its ability to facilitate nodal signaling. *J. Biol. Chem.* **276,** 37769–37778
44. Watanabe, K., Bianco, C., Strizzi, L., Hamada, S., Mancino, M., Bailly, V., Mo, W., Wen, D., Miatkowski, K., Gonzales, M., Sanicola, M., Seno, M., and Salomon, D. S. (2007) Growth factor induction of Cripto-1 shedding by glycosylphosphatidylinositol-phospholipase D and enhancement of endothelial cell migration. *J. Biol. Chem.* **282,** 31643–31655
45. Shi, S., Ge, C., Luo, Y., Hou, X., Haltiwanger, R. S., and Stanley, P. (2007) The threonine that carries fucose, but not fucose, is required for Cripto to facilitate Nodal signaling. *J. Biol. Chem.* **282,** 20133–20141
46. Calvanese, L., Marasco, D., Doti, N., Saporito, A., D'Auria, G., Paolillo, L., Ruvo, M., and Falcigno, L. (2010) Structural investigations on the Nodal-Cripto binding: a theoretical and experimental approach. *Biopolymers* **93,** 1011–1021
47. Bianco, C., Adkins, H. B., Wechselberger, C., Seno, M., Normanno, N., De Luca, A., Sun, Y., Khan, N., Kenney, N., Ebert, A., Williams, K. P., Sanicola, M., and Salomon, D. S. (2002) Cripto-1 activates nodal- and ALK4-dependent and -independent signaling pathways in mammary epithelial Cells. *Mol. Cell. Biol.* **22,** 2586–2597
48. Whitman, M. (2001) Nodal signaling in early vertebrate embryos: themes and variations. *Dev. Cell* **1,** 605–617
49. Lin, S. J., Lerch, T. F., Cook, R. W., Jardetzky, T. S., and Woodruff, T. K. (2006) The structural basis of TGF-β, bone morphogenetic protein, and activin ligand binding. *Reproduction* **132,** 179–190
50. Aykul, S., and Martinez-Hackert, E. (2016) Transforming growth factor-β family ligands can function as antagonists by competing for type II receptor binding. *J. Biol. Chem.* **291,** 10792–10804
51. Myszka, D. G., Jonsen, M. D., and Graves, B. J. (1998) Equilibrium analysis of high affinity interactions using BIACORE. *Anal. Biochem.* **265,** 326–330
52. Calvanese, L., Saporito, A., Oliva, R., D'Auria, G., Pedone, C., Paolillo, L., Ruvo, M., Marasco, D., and Falcigno, L. (2009) Structural insights into the interaction between the Cripto CFC domain and the ALK4 receptor. *J. Pept. Sci.* **15,** 175–183
53. Korchynskyi, O., and ten Dijke, P. (2002) Identification and functional characterization of distinct critically important bone morphogenetic pro-

tein-specific response elements in the Id1 promoter. *J. Biol. Chem.* **277,** 4883–4891

54. Zawel, L., Dai, J. L., Buckhaults, P., Zhou, S., Kinzler, K. W., Vogelstein, B., and Kern, S. E. (1998) Human Smad3 and Smad4 are sequence-specific transcription activators. *Mol. Cell* **1,** 611–617
55. Francescangeli, F., Contavalli, P., De Angelis, M. L., Baiocchi, M., Gambara, G., Pagliuca, A., Fiorenzano, A., Prezioso, C., Boe, A., Todaro, M., Stassi, G., Castro, N. P., Watanabe, K., Salomon, D. S., De Maria, R., Minchiotti, G., and Zeuner, A. (2015) Dynamic regulation of the cancer stem cell compartment by Cripto-1 in colorectal cancer. *Cell Death Differ.* **22,** 1700–1713
56. He, X. C., Zhang, J., Tong, W. G., Tawfik, O., Ross, J., Scoville, D. H., Tian, Q., Zeng, X., He, X., Wiedemann, L. M., Mishina, Y., and Li, L. (2004) BMP signaling inhibits intestinal stem cell self-renewal through suppression of Wnt-β-catenin signaling. *Nat. Genet.* **36,** 1117–1121
57. Nagaoka, T., Karasawa, H., Turbyville, T., Rangel, M. C., Castro, N. P., Gonzales, M., Baker, A., Seno, M., Lockett, S., Greer, Y. E., Rubin, J. S., Salomon, D. S., and Bianco, C. (2013) Cripto-1 enhances the canonical Wnt/β-catenin signaling pathway by binding to LRP5 and LRP6 co-receptors. *Cell Signal.* **25,** 178–189
58. Bianco, C., Strizzi, L., Rehman, A., Normanno, N., Wechselberger, C., Sun, Y., Khan, N., Hirota, M., Adkins, H., Williams, K., Margolis, R. U., Sanicola, M., and Salomon, D. S. (2003) A Nodal- and ALK4-independent signaling pathway activated by Cripto-1 through Glypican-1 and c-Src. *Cancer Res.* **63,** 1192–1197
59. Townson, S. A., Martinez-Hackert, E., Greppi, C., Lowden, P., Sako, D., Liu, J., Ucran, J. A., Liharska, K., Underwood, K. W., Seehra, J., Kumar, R., and Grinberg, A. V. (2012) Specificity and structure of a high affinity activin receptor-like kinase 1 (ALK1) signaling complex. *J. Biol. Chem.* **287,** 27313–27325
60. Babitt, J. L., Zhang, Y., Samad, T. A., Xia, Y., Tang, J., Campagna, J. A., Schneyer, A. L., Woolf, C. J., and Lin, H. Y. (2005) Repulsive guidance molecule (RGMa), a DRAGON homologue, is a bone morphogenetic protein co-receptor. *J. Biol. Chem.* **280,** 29820–29827
61. Andriopoulos, B., Jr, Corradini, E., Xia, Y., Faasse, S. A., Chen, S., Grgurevic, L., Knutson, M. D., Pietrangelo, A., Vukicevic, S., Lin, H. Y., and Babitt, J. L. (2009) BMP6 is a key endogenous regulator of hepcidin expression and iron metabolism. *Nat. Genet.* **41,** 482–487
62. Samad, T. A., Rebbapragada, A., Bell, E., Zhang, Y., Sidis, Y., Jeong, S. J., Campagna, J. A., Perusini, S., Fabrizio, D. A., Schneyer, A. L., Lin, H. Y., Brivanlou, A. H., Attisano, L., and Woolf, C. J. (2005) DRAGON, a bone morphogenetic protein co-receptor. *J. Biol. Chem.* **280,** 14122–14129
63. Corradini, E., Babitt, J. L., and Lin, H. Y. (2009) The RGM/DRAGON family of BMP co-receptors. *Cytokine Growth Factor Rev.* **20,** 389–398
64. Healey, E. G., Bishop, B., Elegheert, J., Bell, C. H., Padilla-Parra, S., and Siebold, C. (2015) Repulsive guidance molecule is a structural bridge between neogenin and bone morphogenetic protein. *Nat. Struct. Mol. Biol.* **22,** 458–465
65. Hartung, A., Bitton-Worms, K., Rechtman, M. M., Wenzel, V., Boergermann, J. H., Hassel, S., Henis, Y. I., and Knaus, P. (2006) Different routes of bone morphogenic protein (BMP) receptor endocytosis influence BMP signaling. *Mol. Cell. Biol.* **26,** 7791–7805
66. Parenti, A., Halbisen, M. A., Wang, K., Latham, K., and Ralston, A. (2016) OSKM Induce extraembryonic endoderm stem cells in parallel to induced pluripotent stem cells. *Stem Cell Reports* **6,** 447–455
67. Gjidoda, A., Tagore, M., McAndrew, M. J., Woods, A., and Floer, M. (2014) Nucleosomes are stably evicted from enhancers but not promoters upon induction of certain pro-inflammatory genes in mouse macrophages. *PLoS ONE* **9,** e93971